Effects of Hydroxylation and Silanization on the Surface Properties of ZnO Nanowires

C. García Núñez,*[,†] M. Sachsenhauser,[‡] B. Blashcke,[‡] A. García Marín,[†] Jose A. Garrido,[‡] and Jose L. Pau[†]

[†]Grupo de Electrónica y Semiconductores, Departamento Física Aplicada, Universidad Autónoma de Madrid, C/Francisco Tomás y Valiente 7, 28049 Madrid, España

[‡]Walter Schottky Institut and Physik-Department, Technische Universität München, Am Coulombwall 4, 85748 Garching, Germany

ABSTRACT: Silanization is commonly used to form bonds between inorganic materials and biomolecules as a step in the surface preparation of solid-state biosensors. This work investigates the effects of silanization with amino-propyldiethoxymethylsilane on hydroxylated sidewalls of zinc oxide (ZnO) nanowires (NWs). The surface properties and electrical characteristics of NWs are analyzed by different techniques after their hydroxylation and later silanization. Contact angle measurements reveal a stronger hydrophobic behavior after silanization, and X-ray photoelectron spectroscopy (XPS) results show a reduction of the surface dipole induced by the replacement of the hydroxyl group with the amine terminal group. The lower work function obtained after silanization in contact potential measurements corroborates the attenuation of the surface dipole observed in XPS. Furthermore, the surface band bending of NWs is determined from surface photovoltage measurements upon irradiation with UV light, yielding a 0.5 eV energy in hydroxylated NWs, and 0.18 eV, after silanization. From those results, a reduction in the surface state density of 3.1×10^{11} cm^{-2} is estimated after silanization. The current−voltage ($I-V$) characteristics measured in a silanized single NW device show a reduction of the resistance, due to the enhancement of the conductive volume inside the NW, which also improves the linearity of the $I-V$ characteristic.

KEYWORDS: ZnO nanowires, hydroxylation, silanization, surface band bending, contact potential difference, surface photovoltage, X-ray photoemission spectroscopy
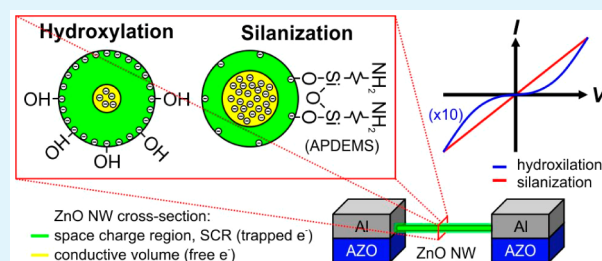
1. INTRODUCTION

Nanowires (NWs) are outstanding materials for the development of gas and biological sensors due to their high surface-to-volume ratio. Besides their excellent optical and electrical properties, one of the advantages of zinc oxide (ZnO) material over other wide band-gap semiconductors is the extensive variety of nanostructures (wires, belts, combs, springs, helixes, rings, cages,[1] tetrapods,[2] etc.) that can be grown by cost-effective techniques such as vapor phase transport (VPT)[3] or solution-phase synthesis.[4] In particular, ZnO-based NWs have been thoroughly studied in the last years due to the facile fabrication procedure and suitable properties for the development of gas sensing[5,6] and UV light detection applications.[7,8] The axial electrical conduction of ZnO NWs is strongly influenced by the negative charges trapped in the sidewall surface and the consequent surface band bending (BB).[7] The adsorption of oxygen at the ZnO surface occurs by trapping free electrons from the NW bulk, thus reducing the electrical conductivity of the NW. Illumination of the NWs with UV light produces an excess of photogenerated holes that are swept to the surface and recombined through the surface levels turning them into neutral states. As a result of this process, oxygen is released from the surface, while trapped negative charges are moved toward the NW core, resulting in a reduction of the space charge region (SCR) width (w_{SCR}) at the surface. After

UV illumination, the recovery time is governed by the trapping times in the surface levels, leading to long reset times.[9,10]

The fabrication of biosensors requires the functionalization of the surface using self-assembled monolayers (SAM) to attach recognition elements such as antibodies, single-stranded DNA, or enzymes. The covalent binding of an organic SAM onto the ZnO surface has been demonstrated using carboxylic acid-,[11,12] thiol-,[13,14] and silane-[15,16] based compounds as linkers. However, most of those works are focused on the chemical modification of ZnO nanoparticles and films, with few studies addressing the surface functionalization of ZnO NWs.[17] In this work, we study the silanization of ZnO NWs after surface hydroxylation by oxygen plasma. The silanization process of hydroxylated ZnO is based on the displacement of alkoxy groups in the silane molecule by the hydroxyl groups (−OH), forming Si−O−Si covalent bonds along the ZnO surface.[18] In general, the formation of the SAM is expected to induce changes in the electronic structure of the surface with different charge-transfer phenomena that can affect the current−voltage ($I-V$) characteristics of the NWs and modify the electrical contact characteristics between NW and electrode.[19]

Contact potential difference (CPD) and surface photovoltage (SPV) measurements allow for nondestructive and contactless investigation of the surface energetics of metals and semiconductors. Whereas CPD measurements performed in dark allow quantification of the work function and surface charge density, SPV provides information about the surface BB. The exposure of the surface to sufficiently intense above-band-gap light leads to the splitting of the quasi-Fermi levels, the screening of surface charges, and the flattening of the surface BB. Therefore, the variation of the CPD value under that kind of illumination provides a direct measurement of the surface BB.

In this work, the ZnO surfaces are analyzed by contact angle measurements, scanning electron microscopy (SEM), atomic force microscopy (AFM), and X-ray photoelectron spectroscopy (XPS) to characterize the surface properties after hydroxylation and silanization. In addition, the effect of the chemical modification on the surface BB is analyzed by CPD and SPV measurements. Finally, $I-V$ characteristics in single ZnO NW devices are analyzed in dark conditions to study the effects of the BB variations on the electrical conduction of the NW. For this characterization, a single NW is aligned and integrated between a pair of conductive electrodes by means of dielectrophoresis (DEP).

2. EXPERIMENTAL DETAILS

A. Material. Vertically aligned ZnO NWs are grown by VPT using a Tempress quartz furnace as thoroughly explained elsewhere.[20] These NWs are synthesized on a Si(100) substrate covered with a 7 nm thick Zn seed layer, using microsized Zn powder (5.5 N purity) and O_2 as solid and gas precursors, respectively, and Ar as carrier gas. Described process is carried out at 900 °C during 180 s, utilizing a mass of Zn powder of 0.5 g, an Ar/O_2 ratio of 1:1, and a total gas flux of 200 sccm, obtaining NWs with diameters between 100 and 500 nm and average lengths of 10 μm as determined by SEM. The resulting samples are analyzed by the techniques mentioned above. For the sake of comparison, a high-purity a-plane ZnO bulk crystal, whose nonpolar surface resembles the NW facet (m-plane),[21] is used as a reference sample in both contact angle and XPS measurements. To prepare a uniform dispersion of NWs for the processing of an electronic device, the NW sample is immersed in ethanol and sonicated for a few seconds. Further processing steps toward the fabrication of a single NW device are described in Section G.

B. Hydroxylation and Silanization of ZnO Surfaces. For the hydroxylation of m-plane (NW sidewall) and a-plane (bulk crystal) ZnO surfaces, both samples are sequentially dipped in hot ethanol, acetone, and ethanol for 5 min, dried in N_2 and finally transferred to an oxygen plasma system (100-E TePla). Once the samples are loaded into the plasma chamber, it is pumped to 0.1 mbar to reduce the influence of contaminants; then, the O_2 gas valve is opened, increasing the residual pressure to 1.4 mbar. Finally, a 200 W power plasma is turned on for 5 min. Plasma treatment removes surface organic leftovers and also promotes the formation of a uniform and stable coverage of −OH on the ZnO surface.[22] The silanization process is performed in a glovebox under Ar ambient (O_2 < 1 ppm and H_2O < 2 ppm) to prevent the oligomerization of APDEMS molecules due to the ambient exposure.[23] The samples are dipped in an aminopropyl-diethoxymethylsilane (APDEMS) solution (0.02 M APDEMS in toluene) and stored in the glovebox for 90 min. After that, samples are rinsed in toluene and isopropanol and dried in N_2.

C. Static Water Contact Angle Measurements. A homemade system is used to investigate the contact angle of deionized water (resistivity, ρ = 18 MΩ cm) droplets on the chemically modified m-plane and a-plane surfaces of NW and bulk reference samples, respectively. Images of 3 μL droplets deposited onto the sample surfaces are acquired using a video camera and later analyzed by image processing software with an accuracy of ±1°.

D. Scanning Electron Microscopy and Atomic Force Microscopy. The morphology of the sample surface is analyzed by SEM (Philips XL30) at 10 kV operation voltage, and AFM images are obtained with a Digital Instruments MultiMode system in tapping-mode using silicon tips at scan frequencies between 0.5 and 0.8 Hz. Image processing, including analysis of step heights, surface roughness, and homogeneity, are performed using Nanoscope and WSxM software.

E. X-ray Photoelectron Spectroscopy. Surface chemical changes are analyzed by XPS, carried out in an ultrahigh vacuum system equipped with a SPECS XR-50 Mg-Anode X-ray source (KE_α = 1253.6 eV) and a SPECS Phoibos 100 hemispherical analyzer with an MCD-5 detector. Experimental data are acquired using a pass energy of 25 eV at a takeoff angle of 0° relative to the surface normal. The examined area is adjusted to ~7 mm^2 using a combination of a mechanical aperture, entrance and exit slits, and electron optics of the analyzer.

For analysis, the raw data are processed by subtraction of linear or Shirley backgrounds and fitted with a Gaussian−Lorentzian mixed function, also called quasi-Voigt function, using the software CasaXPS provided by SPECS GmbH (Berlin, Germany). For the analytical estimation of the relative element molar fraction, first the background accounting for the secondary electrons is removed using a Shirley function, and then element peak is fitted using a Gaussian−Lorentzian mixed function. The integral of the peak is divided by a relative sensitivity factor (R.S.F.), which is characteristic of each element. The R.S.F. for N 1s, C 1s, Zn 2p3/2, and O 1s are 0.42, 0.25, 4.8, and 0.66, respectively.[24]

F. Conductive Potential Difference and Surface Photovoltage. CPD and SPV measurements presented in this work are obtained under ultrahigh vacuum using a Besocke Delta Phi Kelvin Probe S vibrating gold mesh electrode controlled by a Besocke Kelvin Control 07 unit from Besocke Delta Phi GmbH (Jülich, Germany). All the CPD voltages are referenced to the gold work function (Φ_{Au} = 4.7 eV). Illumination is provided by a low-pressure Hg lamp (Benda, Germany).

G. Single NW Device Fabrication. Single NW devices are fabricated by dielectrophoretic alignment through a pair of 100 nm thick Al-doped ZnO (AZO) electrodes defined by photolithography and chemical etching on SiO_2(200 nm)/Si(100) substrates. While an alternating current (AC) signal with an amplitude of 15 V and a frequency of 100 kHz is supplied between coplanar electrodes, a 2 μL droplet extracted from the NW dispersion prepared in Section A is drop-casted onto the electrodes covering the gap area. The electrodes are AC biased until the ethanol is completely evaporated (<1 min). The induced alternating electric field leads to the formation of a dipole moment in the NWs, which are driven toward the high electric field region found at the electrode gap (positive DEP). DEP conditions (amplitude and frequency) have been optimized in previous works to improve the NW alignment efficiency.[25] After alignment, both NW ends are covered with 100 nm thick Al electrodes defined by photolithography and lift-off, aiming to ensure good ohmic characteristics of the NW contacts. The gap width between electrodes needs to be a few microns shorter than the length of the NW for the proper assembly of both sides of the NW on the AZO electrodes. Very narrow distances may jeopardize the final performance of the device by short-circuiting both electrodes during the Al deposition and photolithography steps. For those reasons, the distance between the AZO electrodes is chosen to be 6 μm. As the average NW length is ~10 μm, those electrodes make possible the interelectrode bridge with a few microns difference for the assembly of both NW tips. Then, ZnO NW surface is first hydroxylated and later silanized as explained above. Finally, $I-V$ characteristics of the resultant device are measured at every surface treatment step in dark conditions, aiming to observe variations produced by −OH and APDEMS surface coverages on the electrical conduction of the NW.

3. RESULTS AND DISCUSSIONS

A. Surface Wettability. A 3 μL droplet of deionized water is drop-casted on top of an a-plane ZnO bulk crystal reference

sample and a vertically aligned ZnO NWs sample after hydroxylation and silanization, following the procedures described above. Figure 1a,b shows contact angle images after
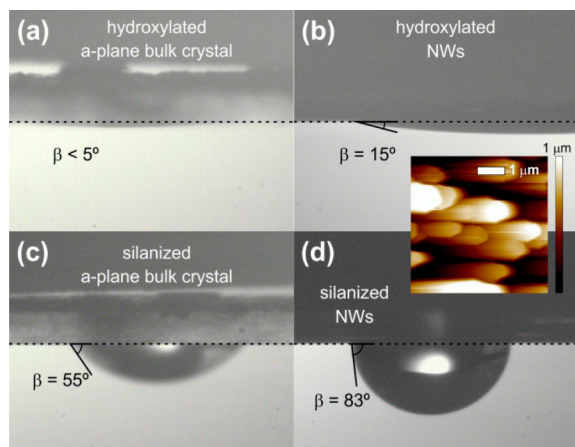

Figure 1. Contact angle measurements of a-plane ZnO bulk crystal and ZnO NW surfaces after (a, b) hydroxylation and (c, d) silanization. (inset) AFM image of vertically aligned ZnO NWs grown on a Si substrate.

hydroxylation, presenting values of ~5° and 15° for the bulk crystal and the NW sample, respectively, and revealing strong hydrophilic behavior, as observed in previous works.[26] After

silanization (Figures 1c,d), the surface turns hydrophobic exhibiting an increase of the contact angles up to 55°, in the a-plane bulk crystal, and 83°, in the NW sample. The contact angle obtained for silanized a-plane bulk crystal sample is close to that value measured in SiC surfaces functionalized by APDEMS.[23] In addition, the higher contact angle observed in the NW sample is associated with the nanostructured morphology of the surface, on which, according to Cassie's model,[27] the droplets can stand, forming a high contact angle.

B. Surface Chemical States. XPS spectra corresponding to N 1s, C 1s, Zn 2p3/2, and surface/bulk O 1s core levels were measured in both a-plane ZnO bulk crystal and ZnO NWs samples after their hydroxylation and silanization. In comparison to the a-plane reference sample (not shown), it is worth noticing that the binding energies for all these elements in the NW sample are shifted by ~3 eV toward larger values due to the geometry of the surface, which induces an extra stopping power when electrons from deeper atoms in the NW are photoemitted. Figure 2a shows XPS survey, and Figure 2b−d shows core levels of ZnO NW sample after its hydroxylation (black) and silanization (red). First evidence of the silanization is the presence of a N peak (Figure 2b), coming from the amine terminal group, and the increase of the C 1s peak (Figure 2c), produced by the hydrocarbon groups in the APDEMS SAM. The origin of the C 1s signal in the hydroxylated sample is likely due to the unintentional C contamination of the ZnO bulk sample during the growth process.[20] After silanization, the C 1s peak increases and shifts 350 meV toward lower binding
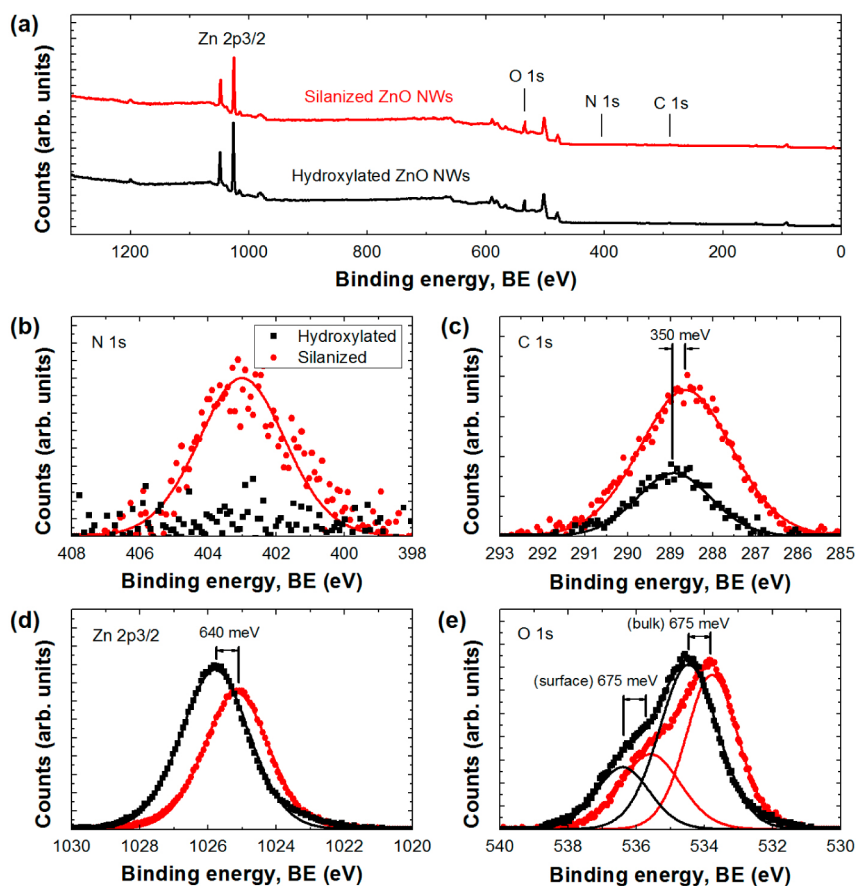
Figure 2. (a) XPS survey spectra of hydroxylated (black) and silanized (red) ZnO NW surfaces. (b) N 1s, (c) C 1s, (d) Zn 2p3/2, and (e) O 1s XPS core-level spectra for ZnO NW surfaces after hydroxylation (black) and silanization (red). Solid lines represent the Gaussian−Lorentzian functions used to fit the signal of each element.

energies. These variations provide another evidence of the presence of the SAM on the ZnO surface associated with the increase of the C molar fraction and the change in the chemical environment of the C atoms.

The attenuation of the Zn photoemission peak observed in Figure 2d is another sign of the SAM formation atop the ZnO surface. Such attenuation can be used to determine the surface coverage and the SAM thickness (d_{SAM}) following the expression (1)[28]

$$d_{SAM} = -\lambda_n \ln\left(\frac{I_{SAM}}{I_0}\right) \tag{1}$$

where λ_n is the photon wavelength at the center of the peak, and I_0 and I_{SAM} are the photoelectron intensity after hydroxylation and silanization, respectively. Expression (1) is used to determine the d_{SAM} in the NW and a-plane bulk crystal samples yielding values of 0.37 and 0.58 nm, respectively. Surface coverage is calculated from those values, using expression (2):

$$\Gamma \text{ (molecules/cm}^2) = \frac{d_{SAM}\rho_{APDEMS}N_A}{M_{APDEMS}} \tag{2}$$

where ρ_{APDEMS} and M_{APDEMS} are the density and molar mass of APDEMS, respectively, and N_A is the Avogadro's constant. From expression (2), the surface coverage after silanization is calculated to be 8.0×10^{13} molecules/cm^2 in the NW sample and 12.6×10^{13} molecules/cm^2 in the a-plane bulk crystal sample. Comparing to the total achievable surface coverage for an a-plane ZnO surface (6.82×10^{14} molecules/cm^2), the resultant surface concentrations correspond to coverages of 11.7% and 18.5%, respectively.

After using the R.S.F. given in Section E in Zn (Figure 2d) and O bulk (Figure 2e) signals, the O(bulk)/Zn ratio calculated for the nonsilanized sample is 1.03, confirming the stoichiometric characteristics of the NWs. After silanization, this factor remains near 1, suggesting that there are no significant changes in the atomic distribution of the bulk caused by the SAM formation.

Figure 2e shows the surface and the bulk O peaks for the NW sample after its hydroxylation and silanization. We first focused on the variation of the surface O. The integral to the Gaussian−Lorentzian fit under the surface O peak is calculated and corrected by both the R.S.F. and the molar factors. For the hydroxylated surface, it must be taken into account that −OH groups bind to the Zn atom under a stoichiometric ratio of 2:1 to form $Zn(OH)_2$ (Figure 3a); therefore, the molar factor is 2. In contrast, silanized samples have APDEMS molecules attached to the ZnO surface (Figure 3b), resulting in a
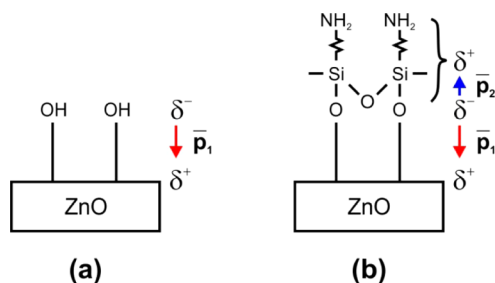
stoichiometry ratio of Zn/O = 1/3 and yielding an effective molar factor of 3. The ratio between the surface O signals in silanized and hydroxylated samples results in 0.9; using this ratio and the surface coverage calculated for APDEMS (8.0×10^{13} molecules/cm^2), the surface coverage of hydroxylated NWs is expected to be $\sim8.9 \times 10^{13}$ molecules/cm^2. This result indicates the efficiency of the initial −OH coverage to promote the attachment of the APDEMS molecules, indicating that most of the −OH groups should be nearly replaced by APDEMS molecules along the ZnO surface.

The successful formation of the SAM on the ZnO surface can also be demonstrated by analyzing the energy shift of the XPS peaks. Figure 2d presents a strong energy shift (640 meV) of the Zn peak toward lower binding energies after the silanization step. This can be attributed to the attenuation of the negative surface dipole, formed after hydroxylation (Figure 3a), by the charges in the APDEMS molecules (Figure 3b). In the hydroxylated samples, the kinetic energy of the photoemitted electrons from the ZnO bulk is reduced due to the influence of the negative surface dipole. Finally, the evidence of the presence of a surface dipole change is also observed in both the O bulk and surface signals, which present a binding energy shift of ~675 meV toward lower binding energies (Figure 2e).

C. Surface Band Bending. CPD measurements are taken to find changes in the surface work function of the NW sample due to the formation of the different surface dipoles after hydroxylation or silanization. Those dipoles can affect the surface BB of the energy bands, which determines the w_{SCR} and the transverse conduction volume along the NW.

Following the hydroxylation treatment, ZnO NW samples exhibited a dark CPD value of $eV_{CPD} = +0.32$ eV (CPD energy plateau observed in the black curve of Figure 4 for times ranged
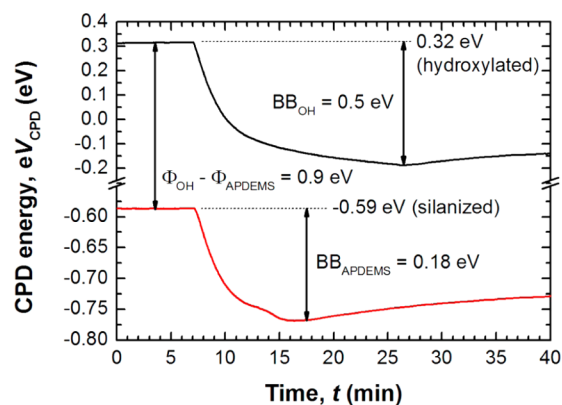
Figure 4. CPD and SPV voltages measured for hydroxylated (black) and silanized (red) ZnO NW samples.

between 0 and 7 min), which corresponds to the voltage necessary to nullify the difference between the Au work function ($\Phi_{Au} = 4.7$ eV) and the surface work function (Φ), defined as the sum of the ZnO work function (Φ_{ZnO}), the surface BB (Φ_s), and the energy step associated with the negative surface dipole induced by the hydroxyl group (Φ_{OH}) (Figure 5a). Therefore, the surface work function of the hydroxylated ZnO NW surface is estimated to be $\Phi = eV_{CPD} + \Phi_{Au} = 5.02$ eV.

For silanized surfaces, the dark CPD values decreases to −0.59 eV (CPD energy plateau observed in the red curve of Figure 4 for times ranged between 0 and 7 min), which means that the local vacuum level is lowered by a negative energy step

Figure 3. ZnO surface dipoles formed after (a) hydroxylation and (b) silanization.
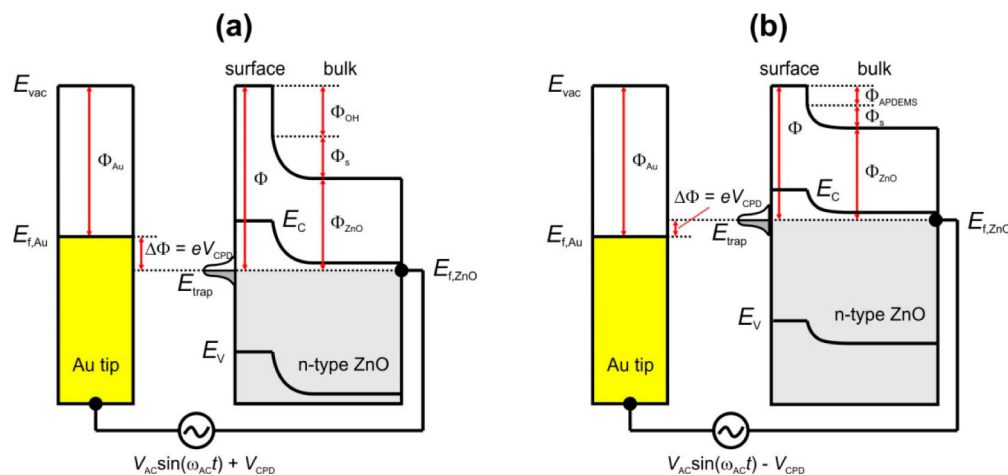
Figure 5. Electronic band structure of (a) hydroxylated and (b) silanized ZnO NW surface for CPD measurements.

induced by the reduction of the surface dipole, due to the charge distribution in the adlayer Φ_{APDEMS} (Figure 5b). Then, the surface work function of the silanized ZnO NW surface is calculated to be $\Phi = eV_{CPD} + \Phi_{Au} = 4.11$ eV. As V_{CPD} is negative in this case, the work function of the silanized surface is lower than the Au work function. This is a direct consequence of surface dipole reduction after silanization also observed in the XPS analysis of the O peak.[23]

During the SPV measurements, the use of a strong illumination above the band-gap energy of ZnO produces BB flattening in hydroxylated and silanized samples, which allows the determination of the Φ_s value. The Φ_s value obtained for hydroxylated and silanized ZnO NW surfaces is found to be 0.5 and 0.18 eV, respectively. Using SPV (Φ_s), CPD results (Φ), and the ZnO work function reported in the literature for as-deposited ZnO ($\Phi_{ZnO} = 3.74$ eV),[29] one can determine the surface dipoles Φ_{OH} and Φ_{APDEMS}, resulting in 0.78 and 0.19 eV, respectively, being in good agreement with XPS results.

Solving the Poisson equation, in thermal equilibrium, for an n-type semiconductor with a single set of discrete surface states of acceptor type, it is possible to obtain the density of surface states (N_{ss}) from the Φ_s expression (3)[30]

$$\Phi_s = \frac{(eN_{ss})^2}{2\varepsilon_{ZnO}\varepsilon_0 N_d} \tag{3}$$

where N_d is the donor density, ε_{ZnO} is the relative permittivity for ZnO ($11\varepsilon_0$), ε_0 is the vacuum permittivity (8.85×10^{-12} C/V m), and e is the electron charge (1.602×10^{-19} C). Assuming an N_d of 1×10^{17} cm^{-3} for VPT ZnO NWs,[31,32] the N_{ss} value can be estimated for hydroxylated and silanized samples using expression (3) and the obtained Φ_s values from CPD and SPV measurements (called BB$_{OH}$ and BB$_{APDEMS}$ in Figure 4), resulting in 7.8×10^{11} and 4.7×10^{11} cm^{-2}, respectively. Therefore, the decrease of the BB obtained after silanization is the result of a reduction in N_{ss} of $\sim 3.1 \times 10^{11}$ cm^{-2} upon attachment of the organic adlayer.

D. Single Nanowire Device Characterization. The surface studies discussed above are completed with the characterization of the electrical conductivity in a single ZnO NW. As the device fabrication method always ends with an organic cleaning to remove the rests of photoresist after the lift-off stage, the described hydroxylation process stabilizes the surface, providing a uniform and stable −OH group coating and setting a reproducible scenario for any further surface

modification that helps the interpretation of the I−V results. Figure 6 shows a layer schematic and an SEM image of the resultant device. In the SEM image (Figure 6b), dashed lines are used to highlight electrodes composed by Al and AZO.
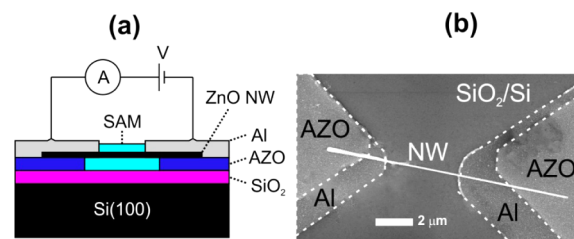
Figure 6. (a) Layer structure schematic and (b) SEM image of the single NW device.

The I−V characteristics of the fabricated devices are measured after every surface treatment (Figure 7). After hydroxylation (black curve), the device presents a current of 0.3 nA at 5 V, which is much lower than those currents measured in the NW devices before any surface treatment (blue curve), and a nonlinear behavior that will be analyzed in depth later on.

Comparing to the hydroxylated device, the silanized device (red curve) presents higher current levels (3 nA at 5 V). To
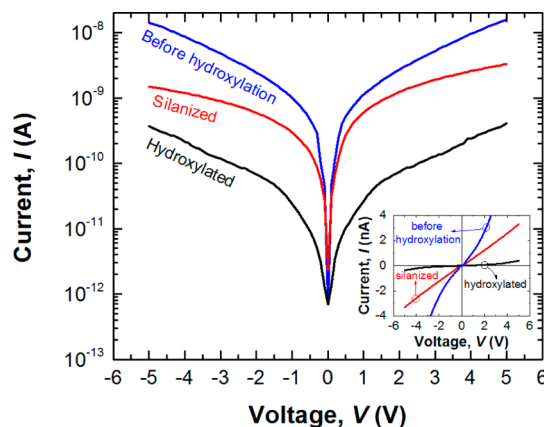
Figure 7. I−V characteristics of a single NW measured before (blue) and after hydroxylation (black) and silanization (red). (inset) I−V curves in linear scale.

understand this change of the current, the w_{SCR} value is calculated at every step from the BB magnitude obtained in SPV measurements (Figure 4) and using expression (4).[21]

$$\Phi_s = \frac{e^2}{2\varepsilon_{ZnO}\varepsilon_0} N_d w_{SCR} \tag{4}$$

The values obtained for w_{SCR} are 78 and 47 nm for hydroxylated and silanized devices, respectively. From Figure 6b, the NW radius (r_{NW}) and length are estimated to be ~60 nm and 4 μm, respectively. Subtracting w_{SCR} from r_{NW}, the hydroxylated device is expected to be fully depleted ($w_{SCR} > r_{NW}$), while the silanized device has a w_{SCR} value lower than the radius. Similar results were obtained in a previous work, where current levels of devices with the same geometry were demonstrated to be directly related by r_{NW} of the ZnO NW.[24] Therefore, those higher current levels measured in the silanized device (or even higher in untreated ZnO NW-based devices) are suggested to be a direct consequence of the SCR narrowing, which means an increase of the conductive volume.

Furthermore, the increase of the conductive volume is also suggested to have a positive effect linearly on the contact such as that observed in the inset of Figure 7, where the $I-V$ curve changes from nonlinear to linear after silanization. Although the free charge emission mainly occurs from the naked surface of the NW, the increase of the free charge density inside the NW can enhance tunneling transport through the contact built-in voltage.[33] Quantum theory predicts that the increase of the carrier population in the NW increases the transmission probability through a potential barrier. This result agrees with a previous study on NWs of different diameters,[24] where it is found that the increase of the conductive volume provokes not only the increase of the conductivity but also the improvement of the linearity of the $I-V$ characteristic. Therefore, devices based on a single NW show nonlinear $I-V$ curves for nearly depleted NWs in contrast to devices with larger diameters and nondepleted volumes. From the results of the present work, it seems that the increase of the free charge inside the volume of a nearly depleted NW through the passivation of surface states can also provoke the improvement of the contact linearity.

4. CONCLUSIONS

ZnO NWs have been successfully functionalized with APDEMS as demonstrated by different techniques such as contact angle measurements, CPD, SPV, and XPS. Silanization makes the surfaces hydrophobic in comparison to the hydrophilic properties shown in the hydroxylated surfaces. The XPS spectra confirmed the attachment of the APDEMS molecules through the presence of N 1s and C 1s peaks, belonging to amine and hydrocarbon groups. The spectra also show a binding energy redshift of both peaks Zn 2p3/2 (640 meV) and O 1s (675 meV) compared to those of the hydroxylated ZnO, evidencing a change in the surface dipole formed atop the ZnO surface. This change of the surface dipole also produces a reduction of the ZnO work function from 5.02 eV (hydroxylation) to 4.11 eV (silanization) as determined by CPD. On the other hand, comparing the width of the surface BB obtained from SPV measurements with the NW axial dimensions, it can be concluded that the hydroxylated NWs are nearly depleted. The $I-V$ characteristics of a single NW are measured integrating the NW between a pair of Al electrodes using DEP. The silanized NW shows larger currents than the hydroxylated NW due to the enlargement of the conductive

volume. Finally, it is observed that the NW silanization improves the linear characteristic of the contact formed between the NW and the Al electrode mainly due to the increase of the total free charge in the NW, which can benefit the output parameters of ion-gated field-effect transistors.

■ AUTHOR INFORMATION

Corresponding Author
*E-mail: carlos.garcia@uam.es.

Notes
The authors declare no competing financial interest.

■ ACKNOWLEDGMENTS

■ REFERENCES

(1) Wang, Z. L. Zinc Oxide Nanostructures: Growth, Properties and Applications. *J. Phys.: Condens. Matter.* **2004**, *16*, R829−R858.

(2) Chen, Z. Zinc Oxide Nanotetrapods. *Nanotechnology* **2004**, *15*, 365−369.

(3) Huang, M. H. Catalytic Growth of Zinc Oxide Nanowires by Vapor Transport. *Adv. Mater.* **2001**, *13*, 113−116.

(4) Greene, L. E.; Yuhas, B. D.; Law, M.; Zitoun, D.; Yang, P. Solution-Grown Zinc Oxide Nanowires. *Inorg. Chem.* **2006**, *45*, 7535−7543.

(5) Sberveglieri, G.; Baratto, C.; Comini, E.; Faglia, G.; Ferroni, M.; Ponzoni, A.; Vomiero, A. Synthesis and Characterization of Semiconducting Nanowires for Gas Sensing. *Sens. Actuators, B* **2007**, *121*, 208−213.

(6) Joshi, R. K. Au Decorated Zinc Oxide Nanowires for CO Sensing. *J. Phys. Chem. C* **2009**, *113*, 16199−16202.

(7) Soci, C.; Zhang, A.; Xiang, B.; Dayeh, S. A.; Aplin, D. P. R.; Park, J.; Bao, X. Y.; Lo, Y. H.; Wang, D. ZnO Nanowire UV Photodetectors with High Internal Gain. *Nano Lett.* **2007**, *7*, 1003−1009.

(8) Suehiro, J.; Nakagawa, N.; Hidaka, S.; Ueda, M.; Imasaka, K.; Higashihata, M.; Okada, T.; Hara, M. Dielectrophoretic Fabrication and Characterization of a ZnO Nanowire-Based UV Photosensor. *Nanotechnology* **2006**, *17*, 2567−2573.

(9) Liu, K.; Sakurai, M.; Liao, M.; Aono, M. Giant Improvement of the Performance of ZnO Nanowire Photodetectors by Au Nanoparticles. *J. Phys. Chem. C* **2010**, *114*, 19835−19839.

(10) Seong, H.; Yun, J.; Jun, H.; Cho, K.; Kim, S. The Transfer of Charge Carriers Photogenerated in ZnO Nanoparticles into a Single ZnO Nanowire. *Nanotechnology* **2009**, *20*, 245201.

(11) Taratula, O.; Galoppini, E.; Wang, D.; Chu, D.; Zhang, Z.; Chen, H.; Saraf, G.; Lu, Y. Binding Studies of Molecular Linkers to ZnO Nanotips. *J. Phys. Chem. B* **2006**, *110*, 6506−6515.

(12) Taratula, O.; Galoppini, E.; Mendelsohn, R.; Reyes, P.; Zhang, Z.; Duan, Z.; Zhong, J.; Lu, Y. Stepwise Functionalization of ZnO Nanotips with DNA. *Langmuir* **2009**, *25*, 2107−2013.

(13) Sadik, P. W.; Pearton, S. J.; Norton, D. P.; Lambers, E.; Ren, F. Functionalizing Zn- and O-terminated ZnO with Thiols. *J. Appl. Phys.* **2007**, *101*, 104514.

(14) Deng, S. Z.; Fan, H. M.; Wang, M.; Zheng, M. R.; Yi, J. B.; Wu, R. Q.; Tan, H. R.; Sow, C. H.; Ding, J.; Feng, Y. P.; Loh, K. P. Thiol-Capped ZnO Nanowire/Nanotube Arrays with Tunable Magnetic Properties at Room Temperature. *ACS Nano* **2010**, *4*, 495−505.

(15) Zeng, T. W.; Liu, I. S.; Huan, K. T.; Liao, H. C.; Chien, C. T.; Wong, D. K. P.; Chen, C. W.; Wu, J. J.; Chen, Y. F.; Su, W. F. Effects of Bifunctional Linker on the Optical Properties of ZnO Nanocolumn-

Linker-CdSe Quantum Dots Heterostructure. *J. Colloid Interface Sci.* **2011**, *358*, 323−328.

(16) Niepelt, R.; Schröder, U. C.; Sommerfeld, J.; Slowik, I.; Rudolph, B.; Möller, R.; Seise, B.; Csaki, A.; Fritzsche, W.; Ronning, C. Biofunctionalization of Zinc Oxide Nanowires for DNA Sensory Applications. *Nanoscale Res. Lett.* **2011**, *6*, 511.

(17) Pauporte, T.; Lincot, D. Electrodeposition of Semiconductors for Optoelectronic Devices: Results on Zinc Oxide. *Electrochim. Acta* **2000**, *45*, 3345−3353.

(18) Allen, C. G.; Baker, D. J.; Albin, J. M.; Oertli, H. E.; Gillaspie, D. T.; Olson, D. C.; Furtak, T. E.; Collins, R. T. Surface Modification of ZnO using Triethoxysilane-based Molecules. *Langmuir* **2008**, *24*, 13393−13398.

(19) Kim, S.; Carpenter, P. D.; Jean, R. K.; Chen, H.; Zhou, C.; Ju, S.; Janes, D. B. Role of Self-Assembled Monolayer Passivation in Electrical Transport Properties and Flicker Noise of Nanowire Transistors. *ACS Nano* **2012**, *6*, 7352−61.

(20) García Núñez, C.; Pau, J. L.; Ruíz, E.; García Marín, A.; García, B. J.; Piqueras, J.; Shen, G.; Wilbert, D. S.; Kim, S. M.; Kung, P. Enhanced Fabrication Process of Zinc Oxide Nanowires for Optoelectronics. *Thin Solid Films* **2014**, *555*, 42−47.

(21) Wang, Z. L. Zinc Oxide Nanostructures: Growth, Properties and Applications. *J. Phys.: Condens. Matter.* **2004**, *16*, R829−R858.

(22) Woll, C. The Chemistry and Physics of Zinc Oxide Surfaces. *Prog. Surf. Sci.* **2007**, *82*, 55−120.

(23) Saddow, S. E. *Silicon Carbide Biotechnology,* 1st ed.; Elsevier: Amsterdam, The Netherlands, 2012.

(24) Schoell, S. J.; Sachsenhauser, M.; Oliveros, A.; Howgate, J.; Stutzmann, M.; Brandt, M. S.; Frewin, C. L.; Saddow, S. E.; Sharp, I. D. Organic Functionalization of 3C-SiC Surfaces. *ACS Appl. Mater. Interfaces* **2013**, *5*, 1393−1399.

(25) García Núñez, C.; García Marín, A.; Nanterne, P.; Piqueras, J.; Kung, P.; Pau, J. L. Conducting Properties of Nearly Depleted ZnO Nanowire UV Sensors Fabricated by Dielectrophoresis. *Nanotechnology* **2013**, *24*, 415702.

(26) Meng, X. Q.; Zhao, D. X.; Zhang, J. Y.; Shen, D. Z.; Lu, Y. M.; Dong, L.; Xiao, Z. Y.; Liu, Y. C.; Fan, X. W. Wettability Conversion on ZnO Nanowire Arrays Surface Modified by Oxygen Plasma Treatment and Annealing. *Chem. Phys. Lett.* **2005**, *413*, 450−453.

(27) Cassie, A. B. D.; Baxter, S. Wettability of Porous Surfaces. *Trans. Faraday Soc.* **1944**, *40*, 546−551.

(28) Johansson, E.; Nyborg, L. XPS Study of Carboxylic Acid Layers on Oxidized Metals with Reference to Particulate Materials. *Surf. Interface Anal.* **2003**, *35*, 375−381.

(29) Kuo, F. L.; Li, Y.; Solomon, M.; Du, J.; Shepherd, N. D. Work Function Tuning of Zinc Oxide Films by Argon Sputtering and Oxygen Plasma: an Experimental and Computational Study. *J. Phys. D: Appl. Phys.* **2012**, *45*, 065301.

(30) Mönch, W. *Semiconductor Surfaces and Interfaces,* 3rd ed.; Springer: New York, 2001.

(31) Li, Q. H.; Liang, Y. X.; Wan, Q.; Wang, T. H. Oxygen Sensing Characteristics of Individual ZnO Nanowire Transistors. *Appl. Phys. Lett.* **2004**, *85*, 6389−6391.

(32) Chang, P. C.; Fan, Z.; Wang, D.; Tseng, W. Y.; Chiou, W. A.; Hong, J.; Lu, J. G. ZnO Nanowires Synthesized by Vapor Trapping CVD Method. *Chem. Mater.* **2004**, *16*, 5133−5137.

(33) Sze, S. M. *Physics of Semiconductor Devices,* 2nd ed.; Wiley: New York, 1981.